Australian Government
Department of Defence
Defence Science and
Technology Organisation

Development of a Thermal Wave Interferometry System for Thin-Film Characterisation

S. Leonard and N. Rajic

Air Vehicles Division

Defence Science and Technology Organisation

DSTO–TR–2760

ABSTRACT

This report describes the development of a thermal wave interferometry system for the characterisation of film thickness. The system furnishes a measurement of the relative phase between a modulated heat flux applied to a thin film by a diode laser and the oscillatory temperature response of the film. The relative phase is then converted to a thickness estimate by means of an inverse solution of the heat diffusion equation. A validation of the facility was performed on an experimental test coupon prepared with paint layers of varying thickness. Estimates of the paint thickness profile furnished by the facility were compared to and corroborated by independent measurements obtained using an eddy current probe and a surface profilometer. The system is shown to resolve variations in paint thickness of less than 1.5 μm.

Published by

DSTO Defence Science and Technology Organisation
506 Lorimer St,
Fishermans Bend, Victoria 3207, Australia

Telephone: (03) 9626 7000
Facsimile: (03) 9626 7999

AR No. 015-431
October 2012

APPROVED FOR PUBLIC RELEASE

Development of a Thermal Wave Interferometry System for Thin-Film Characterisation

Executive Summary

This report describes the development of a Thermal Wave Interferometry (TWI) system for the characterisation of film thickness. The capability addresses the need for a method to assess bondline uniformity for the compact multi-parameter load evaluation (CMPLE) device, a low-cost surface-mounted sensor package with an in-flight strain measurement capability. The device was conceived and developed by the Defence Science and Technology Organisation (DSTO) and successfully tested in-flight on the tail plane of an Australian Defence Force (ADF) Caribou aircraft. However, in validation testing of the device it was revealed that accurate strain readings require that the device be attached with an adhesive bondline that is relatively thin and of uniform thickness. In practice, this can be difficult to achieve even under nominally ideal experimental conditions, raising the need for a reliable method of verifying the thickness and uniformity of the bondline.

As an acutely sensitive method of measuring film thickness, thermal wave interferometry has the potential to provide an effective in situ capability for adhesive bondline metrology. As a first step toward investigating that possibility, a laser-based TWI facility was developed and experimentally validated. The system furnishes a measurement of the relative phase between a modulated heat flux applied by a diode laser and the oscillatory temperature response of the object under inspection. The phase measurement is converted to a thickness estimate by means of an inverse solution of the heat diffusion equation.

A validation of the facility was performed on an experimental test coupon prepared with paint layers of varying thickness. Estimates of the paint thickness profile furnished by the facility were compared to and corroborated by independent measurements obtained using an eddy current probe and a surface profilometer. The system was shown to resolve variations in paint thickness of less than 1.5 μm. Although the main purpose of the facility is to enable the development of an in situ TWI capability for bondline metrology, the facility also offers the potential to assist in the evaluation of coating systems used in military platforms for corrosion prevention and thermal barrier applications.

THIS PAGE IS INTENTIONALLY BLANK

Authors

Stephanie Leonard
Air Vehicles Division

Stephanie is completing a double degree in Computer Science and Electronics Engineering at Swinburne University of Technology. She was on a one year placement with the Smart Structures and Advanced Diagnostics Group as part of the Industry Based Learning Scheme.

Nik Rajic
Air Vehicles Division

Nik Rajic received a B. Eng. (Hons.) in Mechanical Engineering from the University of Melbourne in 1989. He joined Structures Division at the Aeronautical Research Laboratory in 1991 and in 1992 undertook studies at Monash University which led to the completion of a PhD in 1995. He has since contributed to research on fatigue-life extension techniques, thermoelastic stress analysis, thermoplasticity, thermographic nondestructive evaluation and in situ structural health monitoring techniques.

THIS PAGE IS INTENTIONALLY BLANK

Contents

Figures

1 Introduction

This report describes the development of a Thermal Wave Interferometry (TWI) system for the characterisation of thin film properties. The need for such a system was uncovered during an investigation of the compact mult-parameter load evaluation (CMPLE) device [1], a sensor package designed to provide a rapidly deployable operational loads monitoring capability for military aircraft. The device was recently applied in a successful in-flight strain survey of the tail plane of an ADF Caribou aircraft. To function effectively as a strain sensor the device needs to be attached to a host with an adhesive bondline that is relatively thin and of uniform thickness, otherwise biased strain readings can occur. However, in practice, a uniform bondline thickness can be difficult to achieve even under nominally ideal experimental conditions, raising the need for a reliable method of verifying the thickness and uniformity of the bondline.

The installation procedure for the CMPLE device normally results in a bondline thickness of approximately $50\,\mu$m. In general, acoustic methods for thickness measurement based on time of flight are difficult to implement for such short lengths, and acoustic resonance techniques, although sensitive, lack the robustness required for this type of measurement. Within that range of thickness, heat diffusion offers a more practical basis for measurement. The use of TWI to characterise the thickness and thermal properties of thin films is well established [2, 3, 4], and follows the pioneering work of Rosencwaig and Gersho [5] several decades ago. Thermal wave interference occurs in layered structures in response to a modulated heat source and describes a condition where the properties of the interface influence the phase and amplitude of the temperature oscillations at the surface. In the initial work of Rosencwaig and Gersho as well as others [2], the surface temperature oscillations were resolved by means of the photoacoustic method which involves the measurement of pressure variations due to thermal expansion and contraction of the boundary layer of gas (see Figure 1). However, with the widespread availability of low-cost infrared detectors, photothermal radiometry is now preferred over the photoacoustic method for applications involving the measurement of thin film properties [3].

This report describes the development and validation of a TWI facility that employs photothermal radiometry. The main objective of this facility is to provide an experimental platform for the development of an in situ bondline thickness sensor, however the facility has other important potential applications to thin-film material characterisation, one of which is demonstrated as part of an experimental validation process described in the present report.

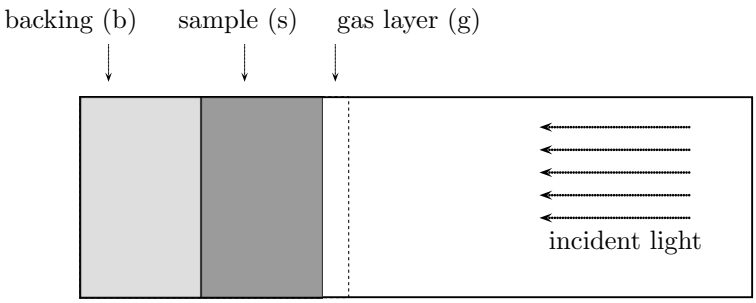

Figure 1: *Layered structure used in the work of Rosencwaig and Gersho.*

2 Theory

Thermal wave interference is fundamentally a result of heat diffusion which is governed by the equation,

$$\frac{\partial T}{\partial t} - \alpha \nabla^2 T = 0, \tag{1}$$

where T represents the change in temperature, t represents time and α is the material thermal diffusivity. Rosencwaig and Gersho [5] show that for the layered structure depicted in Figure 1, modulated laser irradiation of the surface leads to a surface temperature oscillation with the following complex amplitude,

$$\theta = \frac{\beta I_0}{2k_s(\beta^2 - \sigma_s^2)} \left(\frac{(r-1)(b+1)e^{\sigma_s l} - (r+1)(b-1)e^{-\sigma_s l} + 2(b-r)e^{-\beta l}}{(g+1)(b+1)e^{\sigma_s l} - (g-1)(b-1)e^{-\sigma_s l}} \right) \tag{2}$$

where,

$$\begin{aligned} \sigma_s &= (1+j)a_s \\ b &= \frac{k_b a_b}{k_s a_s} \\ g &= \frac{k_g a_g}{k_s a_s} \\ r &= (1-j)\frac{\beta}{2a_s} \\ a_i &= \sqrt{\frac{w}{2\alpha_i}} \end{aligned}$$

Here, β is the optical absorption coefficient for the sample, I_0 is the incident light flux, a_i is the thermal diffusion coefficient of the material and l is the sample thickness. The subscript i can take the values g, s or b for the gas, sample and backing layers respectively, and w denotes the modulation frequency of the incident light.

Equation 2 takes into account the thermal properties of each layer within the structure and also the reflection and transmission of heat at the layer boundaries. Information about the dimensions and thermal properties of a layered structure is contained in the phase

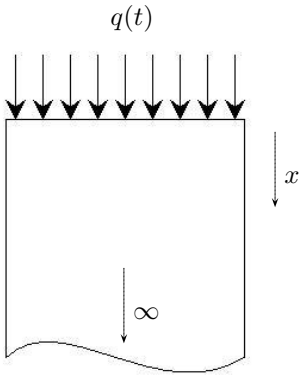

Figure 2: *Semi-infinite solid exposed to a surface heat flux.*

difference between the source modulation and the temperature oscillation at the surface, which is given by the argument of Eqn 2, i.e.,

$$\phi = \arg(\theta), \tag{3}$$

It is important to note that the temperature oscillation at the surface of a semi-infinite body lags the heat source by 45°. The result underpins much of the experimental work described later in this report so is worthwhile elaborating. The result is derived from a harmonic solution to Eqn 1 for the semi-infinite solid shown in Figure 2. For consistency with Ronsencwaig and Gersho, the heat flux $q(t)$ is given the form,

$$q(t) = I_0(1 + \cos(\omega t)). \tag{4}$$

A harmonic solution to the Helmholtz form of the heat diffusion equation can be obtained by a separation of variables,

$$T = \theta(x)e^{j\omega t}, \tag{5}$$

where $\theta(x)$ is the amplitude of the temperature oscillation as a function of penetration depth. Substitution of Eqn 5 into Eqn 2 gives,

$$\frac{d^2\theta}{dx^2} - \frac{j\omega}{\alpha}\theta = 0, \tag{6}$$

which has the general solution,

$$\theta = Ae^{-\sqrt{\frac{j\omega}{\alpha}}x} + B. \tag{7}$$

Notice that $\theta \to 0$ as $x \to \infty$, so $B = 0$, reducing Eqn 7 to,

$$\theta = Ae^{-\sqrt{\frac{j\omega}{\alpha}}x}. \tag{8}$$

The surface boundary condition involves a prescribed flux, i.e.,

$$q = -k \frac{\partial \theta}{\partial x}\bigg|_{x=0}, \tag{9}$$

which fixes the value of the unknown constant A. With further derivation, omitted for brevity, it can be shown that the real part of the surface temperature is,

$$T(x,t) = \frac{I_0 \mu}{2k}\ e^{-\frac{x}{\mu}}\ \cos(\omega t - \frac{x}{\mu} - \frac{\pi}{4}), \tag{10}$$

The term,

$$\mu = \sqrt{\frac{2\alpha}{\omega}} \tag{11}$$

is the thermal diffusion length. This is an important parameter as it provides a length scale for the penetration depth of the temperature oscillations. At the surface of the solid,

$$T(t) = \frac{I_0 \mu}{2k}\ \cos(\omega t - \frac{\pi}{4}). \tag{12}$$

2.1 Effect of Laser Beam Width

The preceding theory assumes one-dimensional (1D) heat flow, which is generally valid where the width of the heat source is large compared to the thermal diffusion length μ. This condition is not always able to be met experimentally, especially when laser irradiation is used (the most common type of source used for TWI), and more so at low modulation frequencies where the thermal diffusion length can be relatively large. Consider for example the inspection of an aluminium sample at a modulation frequency of 1 Hz. Inserting the relevant values into Eqn 11 shows that the diffusion length in this case is approximately 4 mm. In most practical situations that length would exceed the beam width, resulting in strong lateral heat flow and a violation of a key assumption of Eqn 2.

In the present work, the influence of beam diameter on the phase spectrum was examined by means of numerical simulation using the finite element method (FEM). The test case involves an aluminium slab ($\alpha = 52 \times 10^{-5}\,\mathrm{m^2 sec^{-1}}$) exposed to a modulated laser source with a circularly-symmetric Gaussian beam profile. The axisymmetric geometry permits a 2D analysis. At each modulation frequency the simulation time was adjusted to allow transients in the response to extinguish so that the relative phase could be calculated from the steady-state response. Phase spectra were computed for a range of beam diameters. Figure 3 compares these results to theoretical predictions derived from Eqn 2.

The influence of lateral heat flow is clearly significant. As the diffusion length increases relative to the beam diameter the error in the theoretical phase spectrum grows, as expected. The result underscores the need for careful experimental design if analytical expressions such as Eqn 2 are to be used as a basis for analysis. These numerical findings are consistent with experimental results reported by Fabbri and Cernuschi [6]. Although lateral heat flow is an impediment to analysis it does not diminish TWI as a material characterisation tool. Lateral heat flow merely introduces an additional complexity in the phase spectrum, particularly at low modulation frequencies, which needs to be factored into analysis.

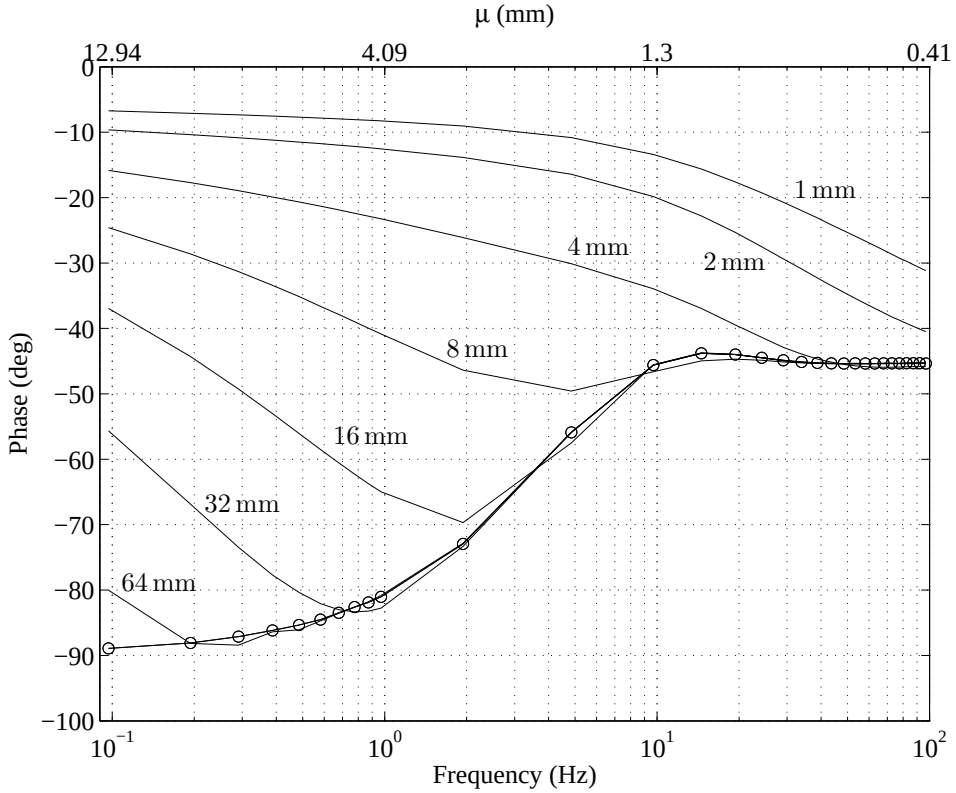

Figure 3: *Phase spectrum as a function of laser beam diameter computed from simulation (FEM). Markers trace the spectrum corresponding to 1D heat flow, as computed from Eqn 2.*

3 Experimental TWI Facility

Since the primary objective of a TWI facility is an accurate measurement of the relative phase between two signals, synchronisation of the source with the response signal is critical. However, any real measurement inevitably involves time delays, which are a potential source of bias that need to be characterised and factored into the computation of relative phase. The steps taken to correct for such factors are discussed in the following.

3.1 Apparatus and Equipment Setup

Figure 4 shows a photograph of the experimental setup. The main components of the apparatus are: (i) an automated micrometer-precision x-y stage on which the sample under investigation is mounted, (ii) a modulated laser source for irradiation of the sample, and (iii) an infrared staring-array camera to measure the induced temperature variations in the sample.

Irradiation of the sample is achieved with a CUBE 660 nm diode laser which has a maximum output power of 100 mW, a beam divergence of approximately 1 milliradian,

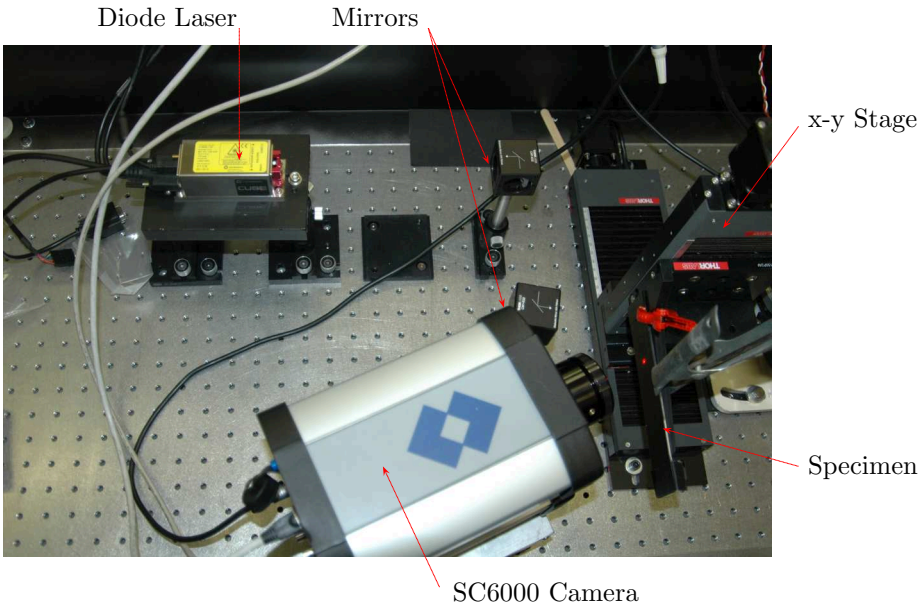

Figure 4: *Experimental apparatus for TWI.*

and a nominal beam diameter of 4.8 mm[1] measured 450 mm from the source. Preliminary tests on the laser revealed that the beam was not circularly symmetric, which is not unusual for diode lasers. Although it is possible to reshape the beam, the process involves a trade-off in beam power, which was not acceptable for the present work where the laser had to be operated at near its maximum power output to produce a satisfactory response signal.

The infrared camera is a commercial FLIR SC6000 unit, equipped with a cryogenically cooled 640×512 staring-array indium antimonide detector with a sensitivity of approximately 17 mK. The camera produces a 16 bit digital output stream which is acquired (nominally) synchronously with a reference signal using custom software [7] on a PC running a windows operating system. The reference in this case is the modulation signal controlling the laser output which was supplied by a stand-alone function generator.

The phase difference between the modulation waveform and the measured temperature response is determined from the argument of the in-phase and quadrature components of the cross-correlation. The correlation sums are computed in real-time which results in rapid convergence. Although the process is effective in rejecting incoherent signals (particularly random Gaussian noise) it is susceptible to systematic phase errors caused by time delays in the acquisition system. As remarked previously, such delays have the potential to bias the computed phase and therefore need to be factored into the cross-correlation process.

[1] the width at $\frac{1}{e^2}$ of the maximum power

3.1.1 Equipment Characterisation

The output data stream from the infrared camera includes an intrinsic time delay associated with the photon integration process, as well as a delay with respect to the skewed acquisition of the reference signal. Essentially, the camera signal represents a photon count over a prescribed integration time τ, a process defined by the following frequency response function,

$$\frac{1}{\tau}\int_0^{\tau} e^{-j\omega t}\mathrm{d}t = \frac{1}{\omega\tau}\Big[j(\cos(\omega\tau)-1)-\sin(\omega\tau)\Big]. \tag{13}$$

The phase delay is then,

$$\phi_\tau(\omega) = \arctan\left(-\frac{1-\cos(\omega\tau)}{\sin(\omega\tau)}\right). \tag{14}$$

In the SC6000, the integration time is set by the user, which means that $\phi_\tau(w)$ is known. Another system delay results from a latency in the acquisition of the infrared data stream and the reference modulation signal which are acquired by separate hardware components in the PC. This latency also results in a frequency dependent phase offset, which for a constant delay, can be expressed as,

$$\phi_{td} = \omega\delta, \tag{15}$$

where td is an acronym for "transport delay" where that delay is denoted by δ which has the unit of time. Unlike the integration time, the transport delay is not known and must be determined experimentally. An apparatus described previously [7] was assembled for that purpose, and is shown schematically in Figure 5. It consists of an area black body which provides a uniform and stable thermal scene that is transformed to a harmonically modulated scene by a pair of linear infrared polarising filters, one of which is fixed while the other rotates at a prescribed frequency maintained by continuous feedback control. The phase of the radiation transmitted through the filter assembly is determined by the relative position of the rotating filter which is tracked by a photodiode/detector unit attached to the assembly, as shown in Figure 5. The arrangement produces an arbitrary phase offset determined by the angular position of the photodetector unit in the plane of rotation. Accordingly, an offset term ϕ_o is added to the phase model, which becomes,

$$\phi = \arctan(-\frac{1-\cos(\omega\tau)}{\sin(\omega\tau)}) + w\delta + \phi_0. \tag{16}$$

It was previously mentioned that the integration time is set by the user, so the value is, by definition, known. However, the authors did not verify whether the prescribed value was precisely implemented by the camera. Any error in the implementation would invariably flow through to the phase model. In that event, τ would need to be treated as unknown and evaluated experimentally. That approach was not taken in the present work where the prescribed value of τ was assumed to be implemented without error. With that

assumption, only two unknowns need to be determined by experiment: δ and ϕ_o. This was achieved by means of linear regression applied to phase measurements adjusted for the integration time, which amounts to minimising the following objective function,

$$\chi = \sum_{i=1}^{N} \left(\hat{\phi}_i - \arctan(-\frac{1-\cos(\omega_i \tau)}{\sin(\omega_i \tau)}) - w_i \delta - \phi_0 \right), \tag{17}$$

over the modulation frequency range $\omega_1 \rightarrow \omega_N$ where $\hat{\phi}_i$ is the measured phase at ω_i.

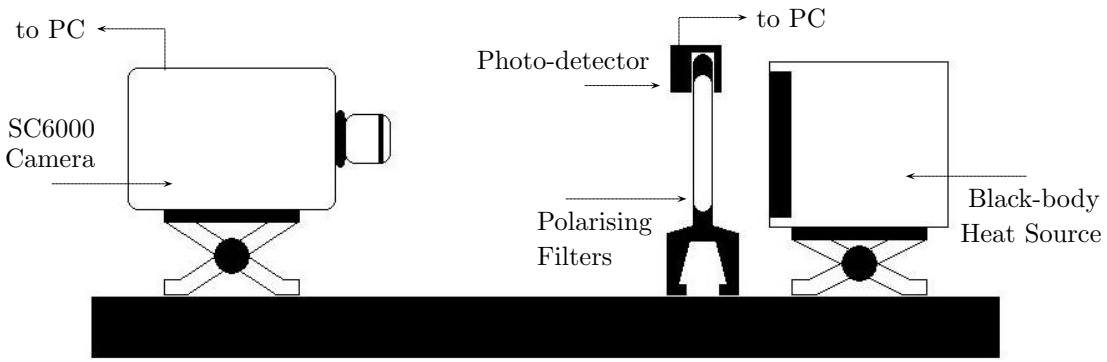

Figure 5: *Experimental setup for SC6000 camera characterisation*

The optimisation was done over a discrete set of frequencies in the range: $1 - 100$ Hz, in increments of 10 Hz. The measured phase at each frequency was derived from a cross-correlation applied over a total of 500 modulation cycles. Further cross-correlation produced no additional improvement in convergence. Table 1 lists δ and ϕ_o values determined for six separate experiments conducted under precisely the same conditions. Both values are seen to vary by almost 10%. The large variance suggests a deficiency in the phase model, possibly caused by the assumption of a constant (time-invariant) transport delay, and a possible problem in the experimental apparatus. A brief investigation of the variability was made, however prior to discussing its outcome it is worthwhile illustrating the effect of the phase corrections defined by Eqn 16 as implemented for the average values of δ and ϕ_o. Figure 6 plots the relative phase spectrum measured for a coated metallic substrate. For this sample, the relative phase should asymptote to $-45°$, which is obviously not achieved, even with all of the corrections in place, however the corrections are seen to significantly reduce the error.

A quick test was done to assess whether the fluctuations were correlated with a change in ambient temperature, which was known to have increased monotonically over the day. The test involved measuring the transport delay and offset at regular intervals across a working day. The values are shown in Table 2, while the transport delay is also plotted in Figure 7. The temperature was not measured, on the basis that the variation was known

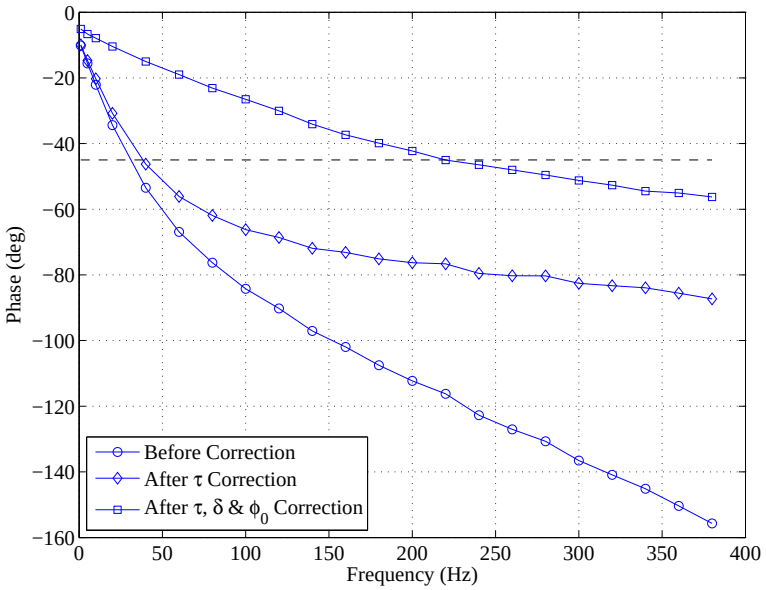

Figure 6: *Variation of phase with frequency with and without correction for system delays.*

Table 1: *Transport delay and phase offset measurements from initial six tests*

δ (ms)	ϕ_0 (°)
-1.1047	4.9143
-1.0992	4.7994
-1.0923	4.4641
-1.0075	4.6062
-1.0099	4.6034
-1.0271	4.8482

to be relatively large ($\approx 5\,^{\circ}$C) and monotonic such that a record of the time was judged an acceptable surrogate. The results in Figure 7 provide no evidence of a correlation.

In the absence of a model for the error, and with limited time available for further investigation, a pragmatic solution was adopted whereby the transport delay is calculated as part of the phase scanning process. The approach requires a reference target with a known phase response on the sample, which can be achieved by including a surface layer with a thickness that is some factor larger than the thermal diffusion length, such that the phase difference between the surface response and the source modulation approaches 45° (see Equation 12). Clearly, a check is required to ensure the beam width is large enough to ensure that lateral heat flow at the point of measurement is negligible.

A test was conducted to determine the extent of variation in the system transport delay as a function of frequency. A metallic sample was coated in a layer of matt black paint $\approx 477\,\mu$m thick[2], which is approximately 2.3 times the thermal diffusion length at a 1 Hz modulation frequency - i.e. the coating can be assumed thermally thick. In addition,

[2]as measured using an eddy current probe

Table 2: *Transport delay and phase offset measurements from time dependency tests*

Time	δ (ms)	ϕ_0 (°)
09:22	-1.0050	4.4240
09:59	-1.0140	4.7988
10:42	-0.9947	4.5829
11:13	-0.9862	4.5692
11:49	-1.0169	4.0517
13:59	-1.0189	4.0359
14:35	-0.9844	4.2030
15:10	-1.0057	4.8313
15:46	-1.0196	4.0461
16:30	-1.0022	4.5562

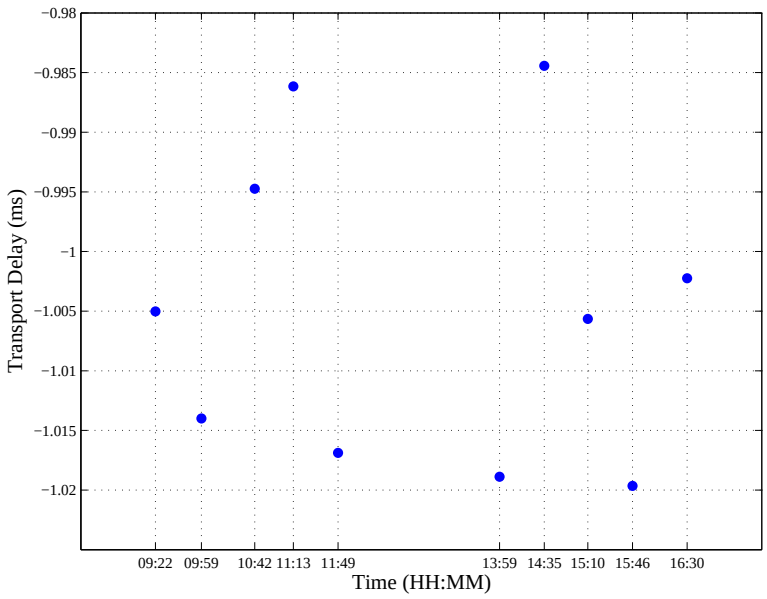

Figure 7: *Variation in SC6000 transport delay with time of test.*

the diffusion length is small relative to the laser beam width ($\approx 4.8\,\text{mm}$) so the assumption of one dimensional heat flow should be well met. The transport delay value required to achieve a relative phase measurement of $-45°$ was recorded for modulation frequencies in the range: $1-200\,\text{Hz}$. These values are shown in Figure 8. The result raises more questions than it answers. One of the concerns relates to the strong frequency dependence. This suggests a variable latency in the acquisition of the separate infrared data and modulation waveform data streams and essentially vindicates the in situ calibration approach. The second concern relates to the fact the asymptotic transport delay differs significantly from the value determined using the calibration apparatus. The reason is unclear and points to the need for further work on addressing this issue. Despite these unresolved questions, it was decided to proceed with an evaluation of the system in measuring film thickness on

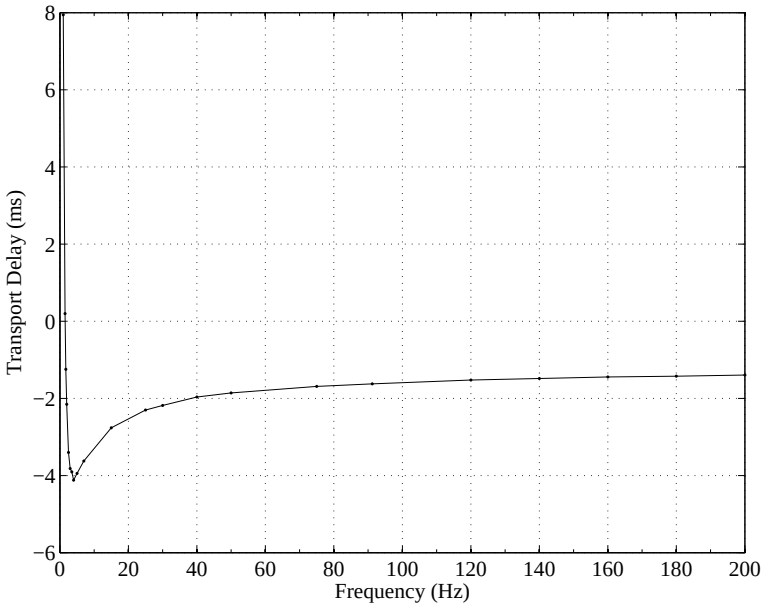

Figure 8: *Variation in SC6000 transport delay with frequency.*

a prepared test sample.

4 Paint Thickness Profiling

Although one of the key objectives of the experimental TWI facility is to furnish a basis for the measurement of adhesive bondline thickness, that particular problem involves several factors that make it a relatively poor test case for a preliminary experimental validation of the facility. Instead, a slightly simpler test case was conceived that has important similarities to the original problem. The case entails the measurement of thickness variations in a paint coating on a metallic substrate. It is attractive for the following reasons. Firstly, as a surface coating, relatively good control is available on the layer thickness, which allows it to be closely matched to the bondline thickness in a typical CMPLE installation. Secondly, independent verification of the layer thickness is relatively straightforward since access to the layer is unfettered. Finally, the thermal diffusivity of the paint chosen for the exercise is similar to that of epoxy, ensuring that the interference behaviour is broadly representative of that in the original problem.

4.1 Measurement of Paint Thermal Diffusivity

A measurement of paint thickness by means of thermal wave interference requires an a priori knowledge of the diffusivity. Flash Thermography (FT) was used to determine the thermal diffusivity of the paint used in the validation exercise. The paint is an RS matte black heat radiator paint commonly used for specimen preparation in thermographic nondestructive inspection and thermoelastic stress analysis applications. A

through-transmission configuration was adopted for consistency with Parker's [8] flash method, whereby one side of the specimen is exposed to a pulsed heat source while the rise in temperature on the opposite side is recorded. In order to produce a paint film that could be inspected this way, a carrier was prepared consisting of a rectangular sheet of cardboard with three circular apertures each covered by a paint film of different thickness, as shown schematically in Figure 9. The films were created by spraying paint onto a thin layer of polyethylene which was carefully removed from the carrier once the paint had dried. The thickness of each layer was measured using an eddy current probe. Measurements were taken at several positions on each layer and averaged, yielding thickness values of $45.85\,\mu\mathrm{m}\,(\mathrm{L}_1)$, $94.71\,\mu\mathrm{m}\,(\mathrm{L}_2)$ and $160.25\,\mu\mathrm{m}\,(\mathrm{L}_3)$.

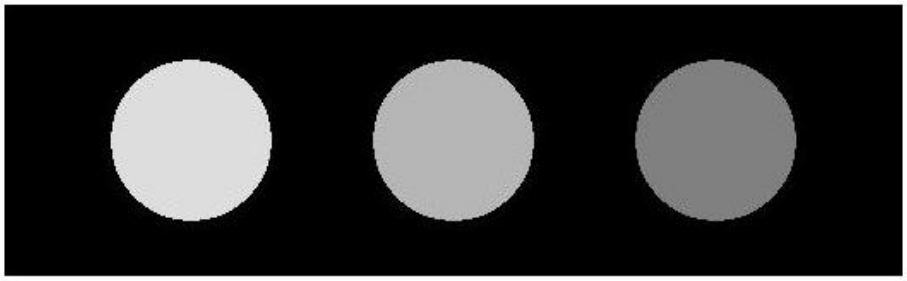

Figure 9: *Schematic of specimen prepared for thermal diffusivity measurement.*

Parker's method appears straightforward, however it assumes a thermal impulse response, which for a very thin object is difficult in practice to achieve. The problem is illustrated in Figure 10, which compares the output of the discharge tube, as measured by a PbSe/Si photo-detector, with the rear-face temperature response for the three layers. The duration of the flash output is not negligibly short, although a reasonable approximation is achieved for the thicker paint layer L_3.

Parker's method can be modified to accommodate a forced response by convolving the known source profile with the impulse response, however in the present study a different approach was taken that produces, in effect, the same result. The known source profile was applied in an FEM simulation to generate a temperature response which was applied in an optimisation process where the thermal diffusivity was varied with the objective of minimising the least-squares error between the measured and modelled response. The minimum error was found to correspond to a value of $1.25 \times 10^{-7}\,\mathrm{m^2 s^{-1}}$, which accords with values published elsewhere for similar paints [9]. Figure 10 shows excellent agreement between the measured response and simulations based on that value, particularly in the early stages of the response when through-thickness diffusion is the dominant heat-transfer mechanism. Note that the peak in the temperature response marks a switch from conduction to convection and radiation dominated heat transfer, which explains the discrepancy that develops between the measured and modelled response for the thin sample as time progresses. The objective function was windowed to exclude that portion of the response so this discrepancy does not effect the estimate obtained for α.

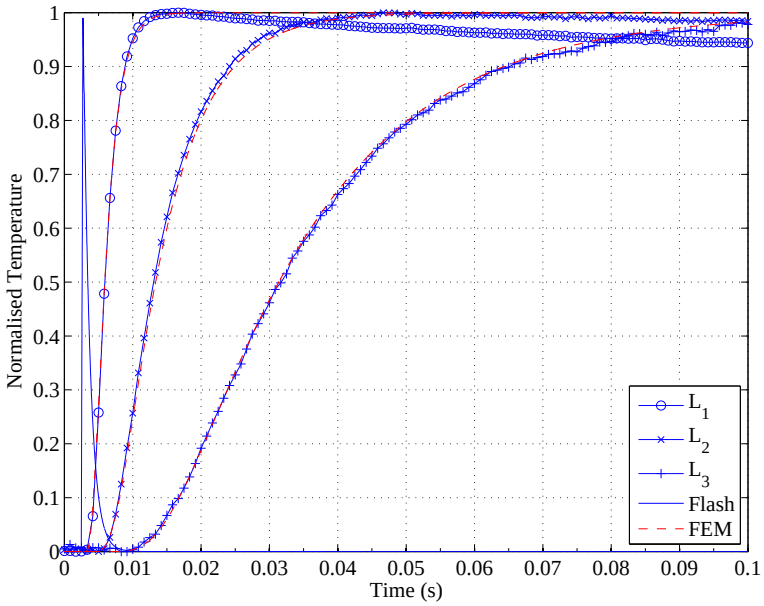

Figure 10: *Flash profile, temperature traces recorded for* L_1, L_2 *and* L_3, *as well as corresponding FEM simulations for the optimal value of* α.

An estimate for the thermal diffusivity was also derived using Parker's method by inserting the half-maximum rise-time (denoted by $t_{\frac{1}{2}}$) for the thin layer response into the expression [8],

$$\alpha = \frac{1.38L^2}{\pi^2 t_{\frac{1}{2}}}. \tag{18}$$

An estimate of $8.9 \times 10^{-8}\,\mathrm{m^2 s^{-1}}$ is obtained, which differs from the optimised value by almost 30%, reinforcing the need to consider the duration of the flash in the diffusivity calculation.

4.2 Non-contact Measurement of Paint Thickness

To facilitate an experimental evaluation of the performance of the facility in characterising film thickness, a test specimen was produced with a coating of the matte black radiator paint described in the previous section. The substrate was a 1.6 mm thick rectangular coupon of Al2024, roughly 150×40 mm in size. A stepped coating thickness profile was produced by applying the paint as an aerosol in multiple passes where strips approximately 30 mm wide were masked once the desired number of paint layers had been applied. The end result is shown schematically in Figure 11. An eddy current probe was used to measure the coating thickness for each strip. Probe measurements were taken at several randomly selected points within each strip and a mean and variance calculated, which are listed in Table 3. Note that the sixth strip was made substantially thicker in order to furnish the "half-plane" reference target required for the transport delay calibration described previously.

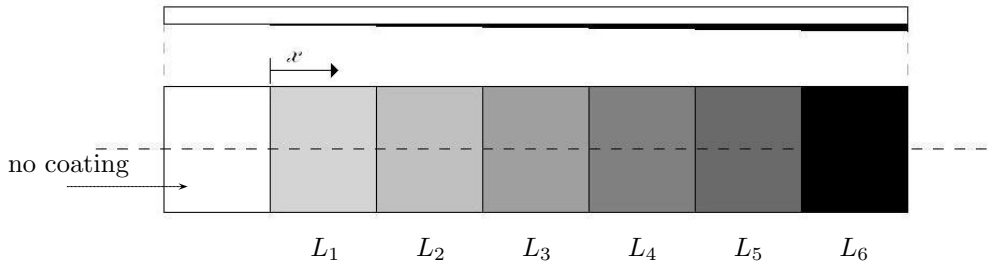

Figure 11: *Plan and front views of Al2024 aluminium alloy specimen with six different paint coating thicknesses (dimensions not to scale).*

Table 3: *Thickness measurements in microns taken with an eddy current probe.*

Thickness	L_1	L_2	L_3	L_4	L_5	L_6
μ	20.44	44.12	74.87	88.07	100.52	476.84
σ	0.97	1.63	2.07	2.64	3.33	7.42
$\mu - \sigma$	19.47	42.49	72.80	85.43	97.19	469.42
$\mu + \sigma$	21.41	45.75	76.94	2.64	90.71	484.26

Interference occurs only when the diffusion length is of the same order as the film thickness which means that the performance of TWI varies significantly with modulation-frequency. Since the material properties of the layered sample are known, as is the thickness profile, at least approximately, Eqn 2 can be used to determine a priori a set of optimal frequencies for inspection. These frequencies were determined by calculating the phase spectrum for a layer thickness one standard deviation above and one standard deviation below the mean measured paint thickness. The two spectra are expected to differ most at precisely the optimal inspection frequency. That approach was applied to strips L_1, L_3 and L_5, yielding frequencies of 4, 7 and 91.2 Hz respectively (Figure 12).

The photograph in Figure 4 shows the sample fixed to the x-y stage in preparation for a scan. A phase profile was formed by measuring the phase at discrete points spaced 2 mm apart along the scan line shown in Figure 11. Each discrete measurement was formed from a cross-correlation involving between 250 and 1000 modulation cycles, depending on the modulation frequency - in general, higher frequencies requiring more cycles. Scans were performed at the three optimal frequencies, as well as at an arbitrary frequency of 30 Hz, which was added for comparative purposes.

The measured phase profiles are shown in Figure 13. Overall, the phase variation across the sample is significant, with a strong discontinuity in phase between each strip. The profile suggests an uneven thickness within some of the strips, which is most evident for L_3. The size of the variation for L_3 was not anticipated given the care taken in preparing the specimen. It is, however, encouraging to note that these variations are largely consistent in form across the four frequencies but amplified for the frequencies predicted by theory to provide optimal sensitivity at the nominal layer thickness - e.g. the variation in phase

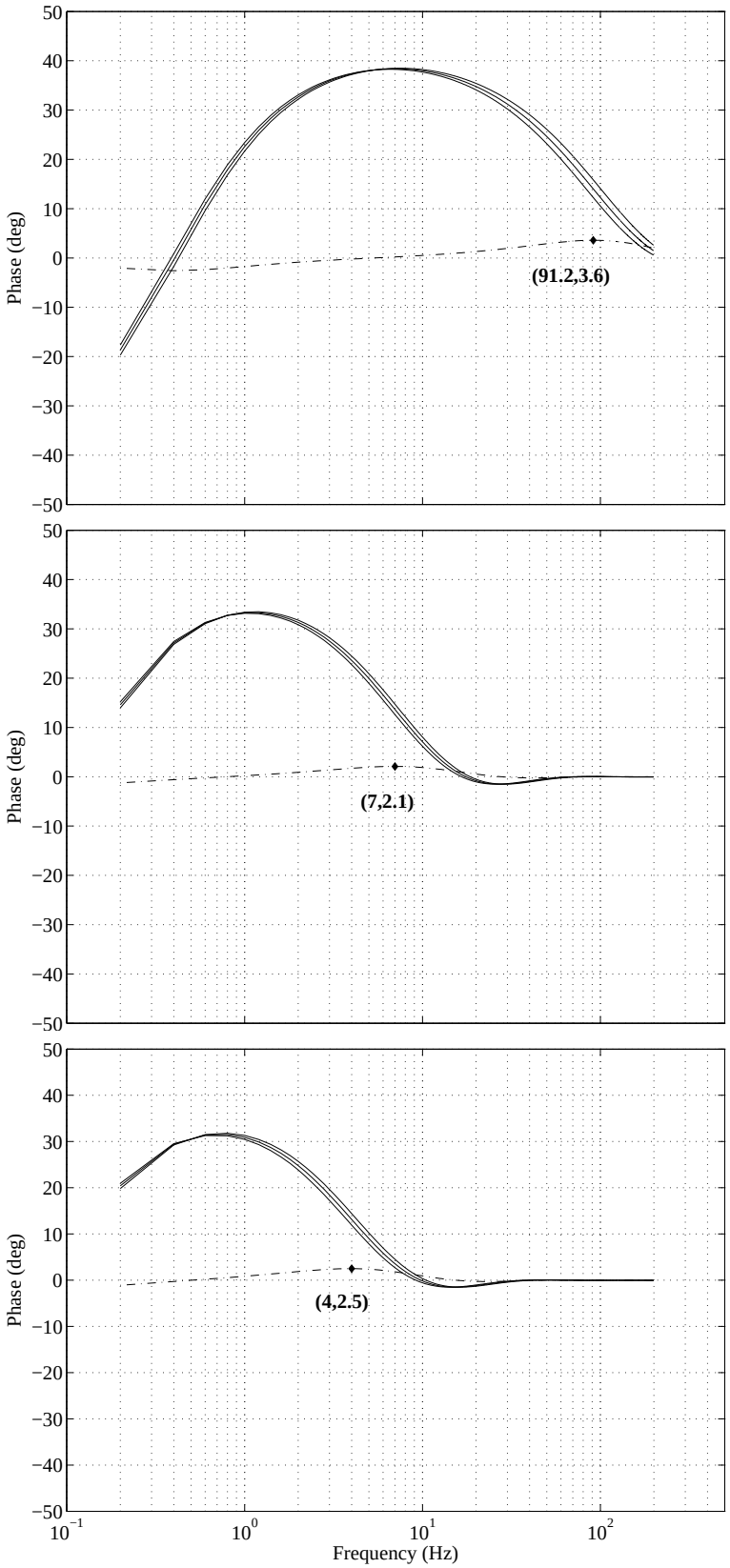

Figure 12: *Calculated phase spectra (solid) and their difference (dashed), revealing optimal modulation frequencies for three different paint thicknesses, L_1 (top), L_3 (middle) and L_5 (bottom).*

across strip L_3 is greatest for a modulation frequency of 7 Hz.

Phase profiles corresponding to the thickness measurements listed in Table 3 were calculated using FEM and Eqn 2. These synthetic profiles are plotted alongside the measured profiles in Figure 14. The agreement between the three sets of results is generally good, noting that the synthetic profiles correspond to an average strip thickness so cannot describe the thickness variations within each strip. Notwithstanding this limitation some important subtleties are captured. Note for instance the 91.2 Hz profile and the small increase in phase from L_2 to L_3. The increase is considered significant as it runs against the overall trend of a monotonically decreasing phase at the lower modulation frequencies. A similar small phase increase against trend is seen for the transition between L_4 and L_5 for the 30 Hz result.

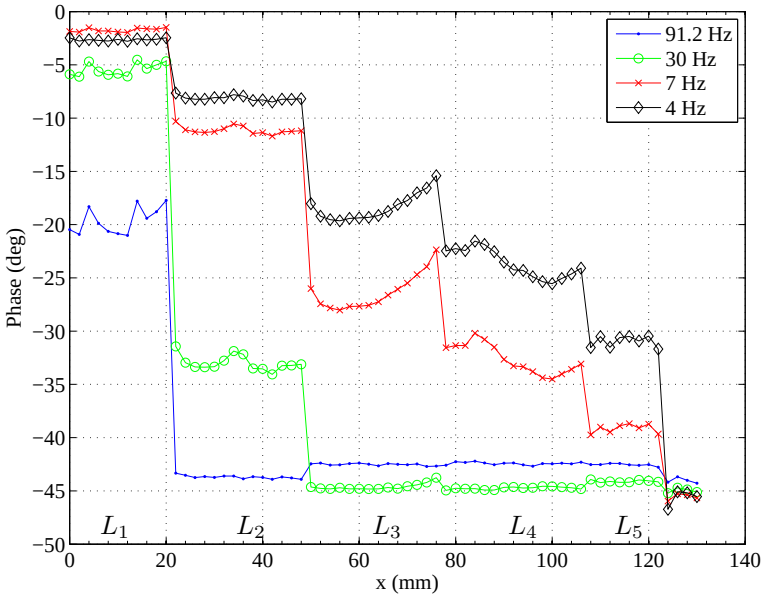

Figure 13: *Phase measurements across the coated sample.*

A more rigorous validation of the experimental result requires that the phase profile produced by the facility be converted to a thickness profile, since this then allows a comparison to be made against independent measurements of thickness. The two profiles are related through heat diffusion so the conversion requires, in effect, the solution of an inverse mathematical problem, where the model can be furnished by Eqn 2 if the heat flow is largely one-dimensional, or by FEM where lateral heat flow is significant. The latter approach was used in the present study. A Nelder-Mead Simplex optimisation routine applied in Matlab was used to solve the relevant inverse problem. Four thickness profiles were produced, corresponding to the four sets of experimental data. The profile estimates are shown in Figure 15. The thickness profile is of course unique so the ambiguity in these estimates is evidence of error, relating either to the inversion process and more likely deficiencies in the experimental data. Some of the error is easily explained. For example, the absence of a profile in the 91.2 Hz result probably reflects weak interference caused

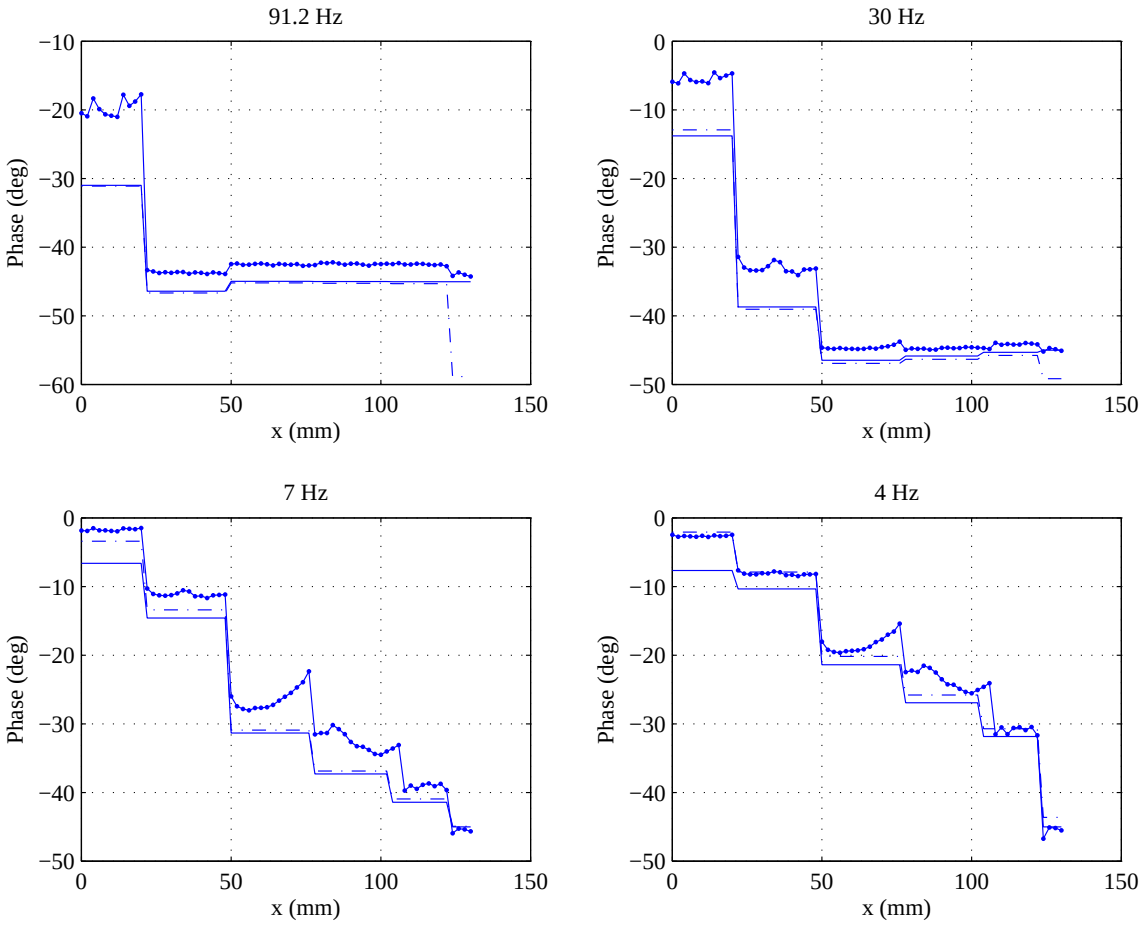

Figure 14: *Comparison between measured (markers), FEM (dashed line) and theoretical (solid line) phase profiles.*

by the short diffusion length at this frequency relative to the layer thickness, which is supported by the largely consistent behaviour in the measured phase profile within the same region. The discrepancy in the 30 Hz result is similarly explained, noting that the erroneous behaviour occurs over a smaller range of coating thickness relative to the 91.2 Hz result, consistent with deeper penetration at the lower frequency. Elsewhere, the discrepancy between profiles is much smaller and mostly characterised by a relatively small offset in the profile which is otherwise consistent.

As none of the modulation frequencies furnish a valid thickness profile across the entire sample it was decided to assemble a complete profile from the results corresponding to the frequency optimised for the particular region, i.e. the profile at 91.2 Hz was selected for L_1, the profile at 7 Hz was used for L_3 and the profile at 4 Hz was chosen for L_5. As the nominal thicknesses of L_4 and L_5 are similar, the profile at 4 Hz was also used for L_4. The profile at 30 Hz was used for L_2 on the basis that that frequency sits between the optimal frequencies determined for the strips to either side.

A further independent measurement of the paint thickness profile was obtained using

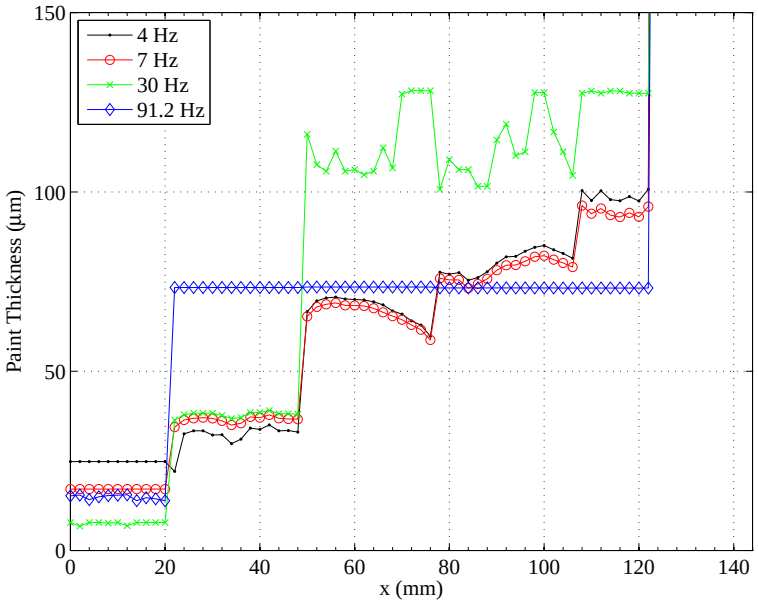

Figure 15: *Paint thickness profiles generated by FEM for each of the four frequencies.*

a surface texture measuring instrument[3], which we refer to now on as a profilometer. The system uses a tracing arm attached to the drive unit housing via a magnetic bearing. According to the technical specifications of the instrument, it yields a surface measurement accuracy of 0.04 μm. Profiles were recorded along three parallel scan lines, one corresponding approximately to the phase-profile scan line shown in Figure 11, and another two taken along lines 1 mm above and 1 mm below the original. These additional scans were done to compensate for uncertainties in the position of the phase-profile scan line.

Figure 16 compares these independently sourced profiles to the TWI result and the average strip thickness measured using the eddy current probe. Part of the profile for L_5 is omitted as the surface texture measuring instrument was limited in its traversal to 120 mm. The agreement overall is excellent. An important observation here is that the intra-strip variations in the TWI profile also occur in the profilometer scans, proving that these are variations in thickness rather than artefacts of the measurement system. In making that assessment allowance needs to be made for the large scatter in the profilometer scans, which is thought to be noise rather than a physical feature of the coating. Analysis of the scatter shows that it accounts for a standard deviation of approximately 1.5 μm which is an order of magnitude above the nominal accuracy of the device. By comparison, the TWI profile is much cleaner, suggesting a noise floor significantly better than 1.5 μm. There are also some concerning aspects about the performance of TWI. Within the thinnest strip, L_1, TWI furnishes a thickness estimate 20% lower than the profilometer and eddy current probe, which is a significant discrepancy that implicates the system phase error discussed previously.

[3]Mahr MarSurf XC10 system with a MarSurf CD 120 drive unit

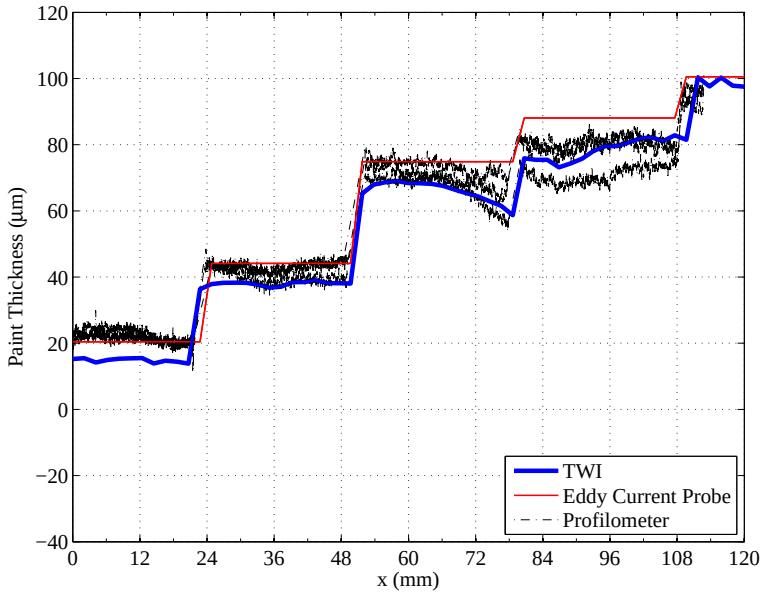

Figure 16: *Comparison of thickness profiles derived from an eddy current probe, a TWI profile estimate, and a surface texture measuring instrument (three separate scans).*

5 General Discussion

An error in the transport delay is known to manifest an error in the system phase output that grows with frequency (see Eqn 15), which was illustrated in Figure 6 where the phase error was obvious for frequencies above 200 Hz. Unfortunately, it was not possible to conclusively determine the phase error within the range of frequencies considered in the test case, however the fact the greatest discrepancy in Figure 16 occurs for the highest modulation frequency, i.e. 91.2 Hz, is consistent with a transport delay error.

There is reason to also question the fidelity of the FEM model used in translating the measured phase values to a coating thickness. In the model, the beam was assumed to have a circularly symmetric Gaussian intensity profile which is known to be an idealisation of the true profile. Figure 17 provides an approximate measurement of the true profile formed by mapping the relative phase across the beam on a thermally thick sample[4]. A contour is included to clarify the asymmetry of the profile. The beam distortion means that the model is likely to have understated the impact of lateral heat flow. The associated phase error should increase as the modulation frequency decreases, as illustrated in Figure 3, so if the effect has had a significant bearing on the results in Figure 16 it should be most apparent for the thicker coatings. Such behaviour was not observed, suggesting the discrepancy at L_1 is unlikely to relate to lateral heat flow and is more probably associated with uncertainty in the system transport delay, as described previously.

In view of the obvious shortfalls in system performance, the results in Figure 16 provide a conservative guide to the full potential of the technique. Given the remarkable quality of the result the potential is evidently large, and gives considerable cause for optimism in achieving the original aim of the facility, which is to provide an experimental platform for

[4] $\mu \to 0$

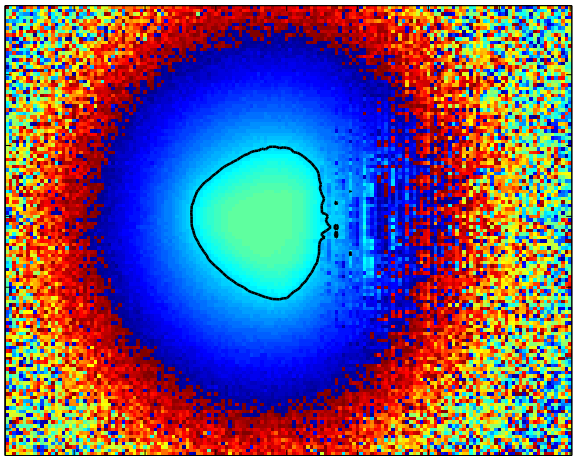

Figure 17: *Asymmetry in the phase across irradiated spot on a thermally thick sample.*

the development of an in situ bondline thickness sensor.

6 Conclusions

This report has detailed the development of a thermal wave interferometry system for the characterisation of film thickness. The system furnishes a measurement of the relative phase between a modulated heat flux applied to a thin film by a diode laser and the oscillatory temperature response of the film. The phase measurement is converted to a thickness estimate by means of an inverse solution of the heat diffusion equation. An accurate measurement of the phase proved difficult to achieve as latencies in the data acquisition system were found to vary with modulation frequency, as well as randomly. Corrections for these latencies were developed and implemented and proved successful in part.

A validation of the facility was performed on an experimental test coupon prepared with paint layers of varying thickness. Estimates of the paint thickness profile furnished by the facility were compared to profiles measured by an eddy current probe and a surface profilometer. Both provided corroboration for key aspects of the TWI result, however evidence was also produced suggesting deficiencies in the approach used to compensate for transport delays in the acquisition system. In view of the considerable scope for improvement in the phase stability of the system, the fidelity of the result was considered remarkable. Work is currently underway on making these improvements, with the anticipation that they should result in a film thickness measurement threshold of well below $1\,\mu$m. Once that is achieved work will proceed on the development of an in situ TWI sensor that can be incorporated into bonded strain-sensing devices such as the CMPLE.

Acknowledgements

The authors are grateful to David Rowlands for his assistance in developing the experimental facility, and to Bruce Grigson for providing the MarSurf XC10 measurements.

References

1. S. Galea and I. Powlesland. Caribou loads flight survey using a rapid operational loads measurement approach. *Materials Forum*, 33, 2009.

2. Jr. C. A. Bennett and R. R. Patty. Thermal wave interferometry: a potential application of the photoacoustic effect. *Applied Optics*, 21(1):49 – 54, 1982.

3. A. Bendada. Sensitivity of thermal-wave interferometry to thermal properties of coatings: application to thermal barrier coatings. *Measurement Science and Technology*, 13:1946, 2002.

4. O. Raghu and J. Philip. Thermal properties of paint coatings on different backings using a scanning photo acoustic technique. *Measurement Science and Technology*, 17:2945, 2006.

5. A. Rosencwaig and A. Gersho. Theory of the photoacoustic effect with solids. *Journal of Applied Physics*, 47(1):64–69, Jan 1976.

6. L. Fabbri and F. Cernuschi. Finite laser beam size effects in thermal wave interferometry. *Journal of Applied Physics*, 82(11):5305–5311, 1997.

7. N. Rajic, S. Weinberg, and D. Rowlands. Development of a low cost thermoelastic stress analysis system. *Defence Science and Technology Organisation, Australia*, DSTO-TR-2164, 2008.

8. C. P. Butler W. J. Parker, R. J. Jenkins and G. L. Abbott. Flash method of determining thermal diffusivity, heat capacity, and thermal conductivity. *Journal of Applied Physics*, 32(9):1679–1684, 1961.

9. N. Rajic. An investigation of the bias caused by surface coatings on material loss evaluation by quantitative thermography. *Journal of Nondestructive Evaluation*, 191(4):141–147, 2000.

DEFENCE SCIENCE AND TECHNOLOGY ORGANISATION DOCUMENT CONTROL DATA	1. CAVEAT/PRIVACY MARKING

2. TITLE	3. SECURITY CLASSIFICATION
Development of a Thermal Wave Interferometry System for Thin-Film Characterisation	Document (U) Title (U) Abstract (U)
4. AUTHORS	5. CORPORATE AUTHOR
S. Leonard and N. Rajic	Defence Science and Technology Organisation 506 Lorimer St, Fishermans Bend, Victoria 3207, Australia

6a. DSTO NUMBER	6b. AR NUMBER	6c. TYPE OF REPORT	7. DOCUMENT DATE
DSTO–TR–2760	015-431	Technical Report	October 2012

8. FILE NUMBER	9. TASK NUMBER	10. TASK SPONSOR	11. No. OF PAGES	12. No. OF REFS
2012/1009595/1	DERP 07/250	CAVD	22	9

13. URL OF ELECTRONIC VERSION	14. RELEASE AUTHORITY
`http://www.dsto.defence.gov.au/publications/scientific.php`	Chief, Air Vehicles Division

15. SECONDARY RELEASE STATEMENT OF THIS DOCUMENT

Approved for Public Release

OVERSEAS ENQUIRIES OUTSIDE STATED LIMITATIONS SHOULD BE REFERRED THROUGH DOCUMENT EXCHANGE, PO BOX 1500, EDINBURGH, SOUTH AUSTRALIA 5111

16. DELIBERATE ANNOUNCEMENT

No Limitations

17. CITATION IN OTHER DOCUMENTS

No Limitations

18. DSTO RESEARCH LIBRARY THESAURUS

Nondestructive testing, Infrared imaging, Infrared sensors, Materials

19. ABSTRACT

This report describes the development of a thermal wave interferometry system for the characterisation of film thickness. The system furnishes a measurement of the relative phase between a modulated heat flux applied to a thin film by a diode laser and the oscillatory temperature response of the film. The relative phase is then converted to a thickness estimate by means of an inverse solution of the heat diffusion equation. A validation of the facility was performed on an experimental test coupon prepared with paint layers of varying thickness. Estimates of the paint thickness profile furnished by the facility were compared to and corroborated by independent measurements obtained using an eddy current probe and a surface profilometer. The system is shown to resolve variations in paint thickness of less than 1.5 μm.